STUDIES IN GEOPHYSICS

Explosive Volcanism: Inception, Evolution, and Hazards

Geophysics Study Committee
Geophysics Research Forum
Commission on Physical Sciences,
Mathematics, and Resources
National Research Council

NATIONAL ACADEMY PRESS
Washington, D.C. 1984

Experimental Studies of Hydromagmatic Volcanism

12

KENNETH H. WOHLETZ *and* ROBERT G. McQUEEN
Los Alamos National Laboratory

ABSTRACT

Hydromagmatic volcanism was modeled in experiments in which thermite melt ($Fe + Al_2O_3$) explosively interacted with water. Several designs were explored using different contact geometries, water-melt ratios, and confinement pressures. The explosions featured ejection of steam and fragmented melt. The modeled volcanic phenomena includes melt fountains (Strombolian), dry and wet vapor explosions (Surtseyan), and passive chilling of flows (submarine pillow formation). The pertinent experimental parameters are: (1) ejection velocities of 20 to 100 m/sec, (2) confining pressures of 10 to 40 MPa, (3) melt ejecta sizes of microns to centimeters in diameter, (4) steam production at temperatures of 100°C to high levels of superheating (300 to 500°C), and (5) ejection modes that are both ballistic and surging flow in a turbulent expanding cloud of vapor and fragments. The results indicate that explosive efficiency is strongly controlled by water-melt mass ratio and confining pressure. Optimum thermodynamic efficiency measured as the ratio of mechanical to thermal energy occurs at water-melt ratios between 0.3 and 1.0. Fragmentation increases with explosive energy and degree of water superheating.

INTRODUCTION

The understanding of explosive volcanism has been limited by the difficulty of documenting many of the physical parameters involved. Visual assessments of the eruption products and their movement, like those detailed by Moore and Rice (see Chapter 10 of this volume), are necessarily distant observations. Only qualitative inferences can be made about the explosion process. Experimental modeling can be used to evaluate the energetics as well as boundary conditions of an eruption in that important parameters such as pressure, temperature, velocity, and density can be measured.

Volcanic explosions are the result of explosive expansion of volatile materials. Two end-member processes account for the origin of these volatiles: (1) *hydromagmatic* (hydrovolcanic) processes in which hot magma interacts with external water at or near the surface of the Earth, producing vapor explosions (see Figure 12.1), and (2) *magmatic* processes in which volatiles in the melt (dominantly H_2O) exsolve and explosively fragment the magma by rapid decompression. These two processes may operate simultaneously during an eruption if the magma composition and environmental factors permit.

Experiments (Wohletz and Sheridan, 1981, 1982; McQueen and Wohletz, in preparation) reviewed in this paper provide information on hydromagmatic processes. Although experimentation on hydromagmatic volcanism has just begun, considerable work on vapor explosions has been done in the field of nuclear reactor safety (Sandia Laboratories, 1975). These studies build on previous work aimed at understanding disastrous industrial explosions in which molten metal has come into accidental contact with water (Lipsett, 1966). Such explosions are termed *fuel-coolant interactions* (FCIs), and their behavior has been studied in small-scale laboratory experiments (Board *et al.*, 1974; Peckover *et al.*, 1973). Recent work (Buxton and Benedict, 1979, Corradini, 1980; Nelson and Duda, 1981) dealing with theoretical and laboratory investigations of nuclear reactor systems also lends considerable insight into volcanic processes.

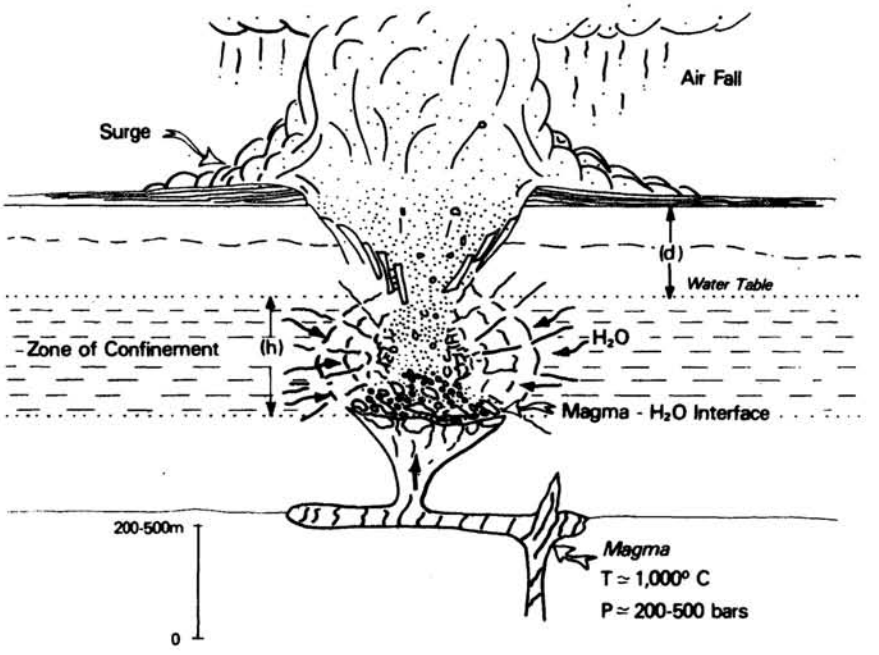

FIGURE 12.1 Diagrammatic cross section of a hydrovolcanic eruption in which magma interacts with near-surface groundwater. The interaction fragments the magma and country rock, vaporizes the water, and produces steam explosions that excavate a crater and eject tephra. Scale shown is for maar volcanoes of typical size.

GEOLOGIC BACKGROUND

Thomas Jaggar (1949) was an early advocate of the idea that many volcanic eruptions are the result of hydromagmatism. The importance of this mechanism to explosive volcanism was not totally appreciated, however, until the pyroclastic surge deposits from these eruptions were recognized for their widespread occurrence (Moore, 1967; Fisher and Waters, 1970; Waters and Fisher, 1971). Classical terms for eruptive styles of hydromagmatic volcanoes include (1) *Surtseyan* (Thorarinsson, 1966), exemplified in the explosive birth of the island Surtsey near Iceland, where repeated blasts deposited numerous layers of ash from base surges and ash falls (Figure 12.1); (2) *Strombolian* (Walker and Croasdale, 1971; Chouet *et al.*, 1974), typified in the growth of the Stromboli Volcano in the Mediterranean, where limited interaction of seawater with magma and magmatic gases produced low-energy bursts forming cinder cones; and (3) *submarine* eruptions where lava is extruded passively on the ocean floor with little or no explosive interaction with water (see Figure 12.2).

EXPERIMENTAL APPROACH

In the experiments described here the volcanic environment was simulated by bringing molten thermite into contact with water. The objective was to determine the parameters that control explosivity. Explosions occur when water vaporization at extreme P and T results in rapid conversion of the melt's thermal energy into mechanical energy.

Thermite

The process of thermite converting to melt arises through a highly exothermic oxidation-reduction reaction of a metal and metal oxide. The process has many applications, the most familiar of which relate to welding. The following physical properties of thermite resemble those of basaltic magmas and thus make it useful for our modeling:

1. the reaction temperature is greater than 1000°C,
2. viscosity is in the range of 10^3 poise,
3. density is 3 to 5 g/cm^3,
4. the melting yields a mixture of crystals and liquid within the T and P of investigation, and

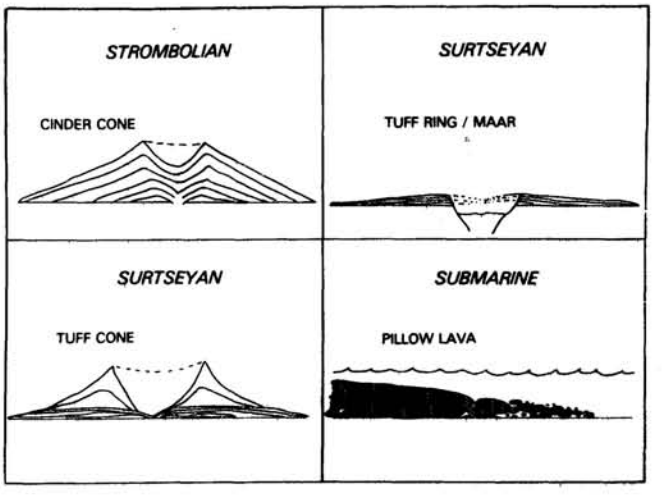

FIGURE 12.2 Land forms produced by four principal modes of hydrovolcanic activity. The layering of pyroclastic material illustrated results from periodic eruption pulses, avalanching of debris, and base surge and emplacement. Surtseyan tuff rings result from more highly explosive eruptions than do Surtseyan tuff cones, hence their lower profiles.

5. the mixture flows over a surface in a manner similar to basalt.

There are limitations, however, that must be considered: the enthalpy of molten thermite (ΔH = 877 cal/g) is about three times that of basalt; the melting temperature may exceed 2000°C, whereas basalt typically melts at 1200°C; and the chemical composition of the thermite is unlike that of basalt. Because of large enthalpy of thermite, addition of oxides such as silica to the system produces a melt chemistry that more closely matches that of a basalt. The thermite reaction is

$$Fe_3O_4 + 8/3\ Al = 4/3\ Al_2O_3 + 3\ Fe + \Delta H. \quad (12.1)$$

After the melt contacts water, additional enthalpy results from the spontaneous oxidation of Fe, dissociation of H_2O, and subsequent burning of H_2. This effect is minor, however, and occurs after the initial explosive interaction. Because the thermite reaction is essentially adiabatic and occurs at low pressures, the total internal energy is equal to the system's enthalpy.

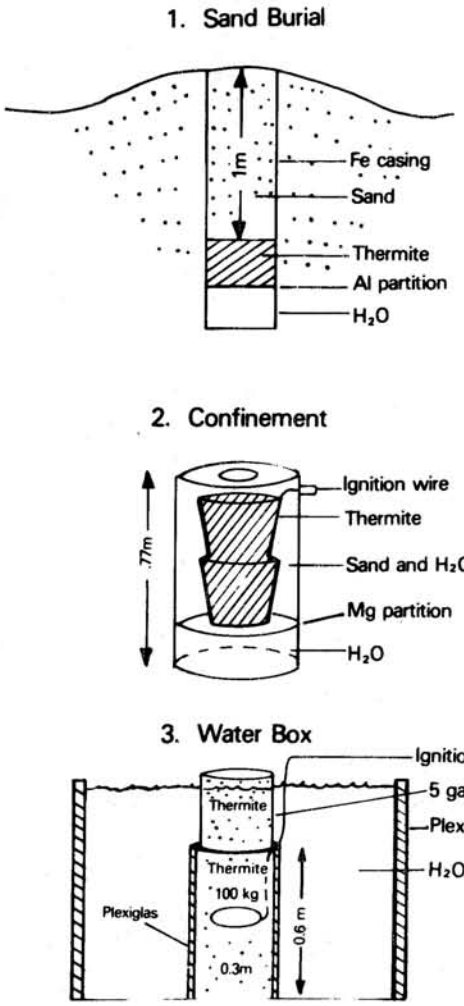

FIGURE 12.3 Three experiments for simulating volcanic eruptions.

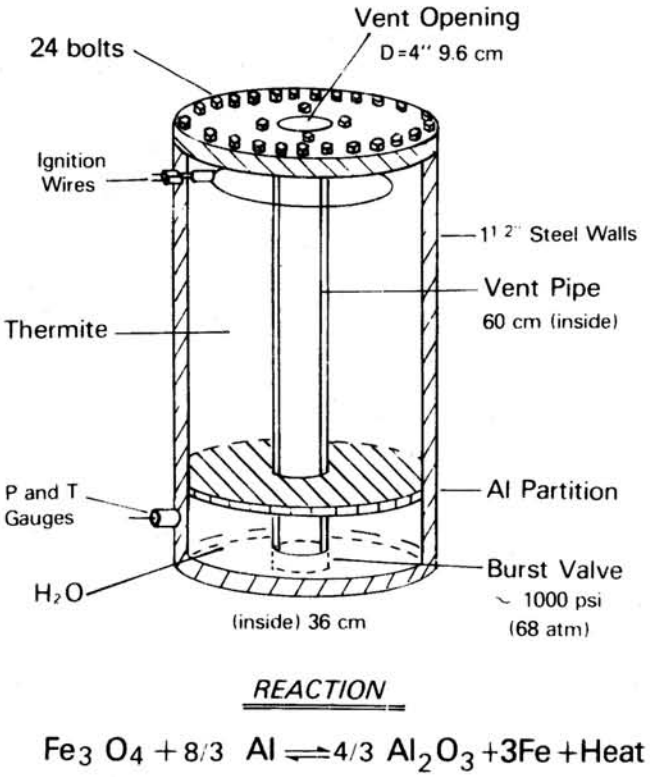

FIGURE 12.4 A fourth experimental apparatus designed to measure P and T during eruption.

Design

Four experimental setups have been used to simulate different volcanic environments (see Figure 12.3). In the first configuration, the thermite was buried in sand to produce an explosive magma model. A second design gave further confinement by enclosing thermite and water in a sealed steel cylinder with a burst valve at the top. In the third design a large (1 m^3) box with a Plexiglas side was filled with water and enclosed another plexiglas tube filled with thermite. This design allowed some visual assessment of the melt-water interaction. The fourth model, illustrated in Figure 12.4, allowed more precise documentation and control of experimental variables. The aims of this design were as follows:

1. To ignite the thermite from the top down so as to ensure a completely molten state prior to contact with water. In the setup an aluminum partition separating the thermite and the water must be melted for contact to occur.
2. To make the hydrostatic head of the melt force contact with water in the same way that basalt rising under a pressure head contacts surface water.
3. To simulate near-surface conditions by setting the burst valve at about 1000 psi (7 MPa).

4. To design the vent such that all of the melt must move through the water compartment during venting. Otherwise, trapped water would expel large amounts of melt above it without the chance for efficient heat exchange. In this way thermite is modeled as magma that had to move through near-surface water during extrusion.

5. To incorporate T and P recorders in the water compartment.

Documentation

High-speed cinematography was used as the primary means of documenting the experiments. Through photography it is possible both to compare the model qualitatively with volcanic eruptions and to measure quantitative features such as velocity, event timing, and ejecta trajectories by frame-to-frame analysis (Figures 12.5 and 12.6).

Pressure measurements made from gauges connected through the steel confinement casing were recorded on strip charts. Three gauges were used—two with a dynamic range from 0 to 5000 psi and one for recording nonpressure-related events. Records show timing for the initiation, duration, and intensity of the melt-water interaction.

Thermocouple records and postexplosion inspection of the confinement chamber provided only limited information. Thermocouple probes inserted into the water compartment measured minimum-temperature rise times and amplitudes for conditions in the zone of interaction. In the postexperiment inspection of the confinement chamber, the degree of melt-water mixing was assessed from the completeness of the chamber evacuation and the size and distribution of the ejecta.

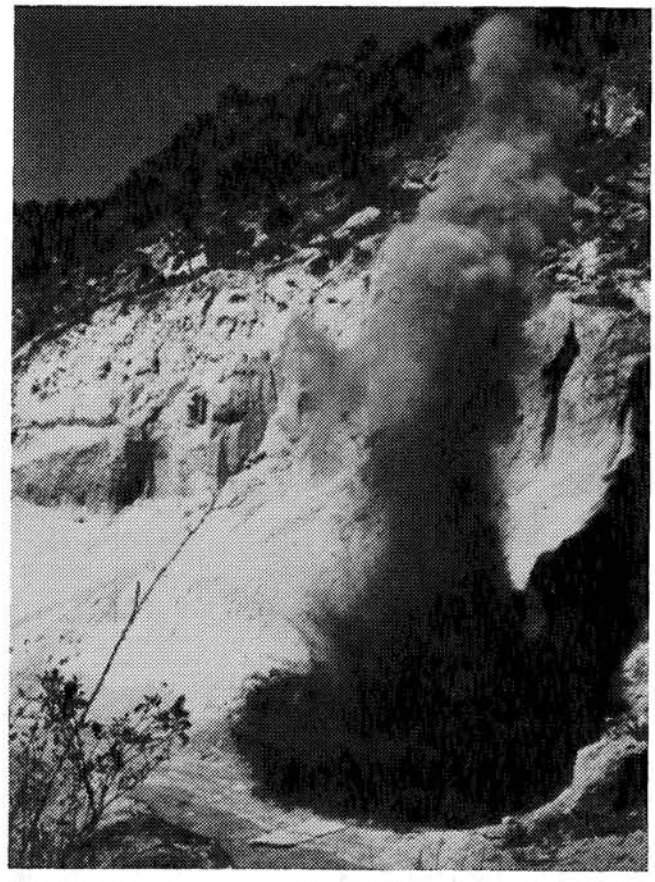

FIGURE 12.5 Experiment 1 (Table 12.1) showing vertical ejection column and horizontally expanding base surge.

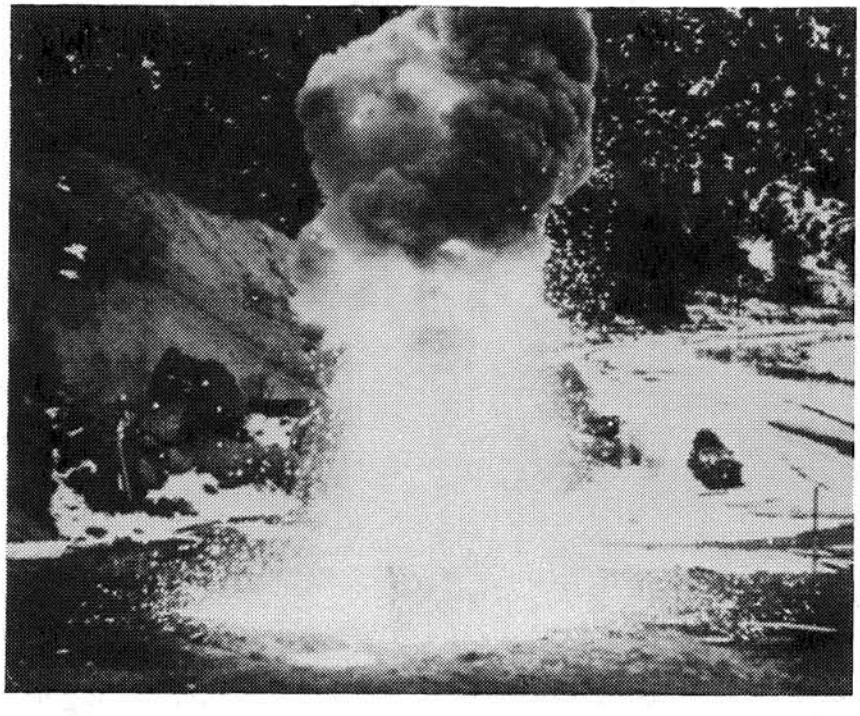

FIGURE 12.6 Water-box experiment in Strombolian activity.

EXPERIMENTAL RESULTS

This paper reviews the first stages of our experimental program; only tentative analyses are reported. The results are divided into three categories: venting phenomena, ejecta characteristics, and pressure histories.

Venting Phenomena

Descriptions of the system and the observed venting phenomena are given in Table 12.1 and Figure 12.7. These are characterized by three independent parameters: degree of confinement, water-melt mass ratio (R), and contact geometry.

The experimental eruption phenomena illustrated in Figure 12.7 are necessarily generalized. Also, no experiment shows just one phenomenon. Their classification is based on the dominant behavior. The most important requirement in this type of modeling is that the mechanism of the experiment be as close as possible to that operating in nature. As discussed earlier, the mechanism is basically the same as that in nature. The experimental explosions bear a remarkable resemblance to volcanic eruptions despite the following limitations: (1) use of a rigid cylindrical vent that directs ejecta vertically; (2) the high temperature of the melt, which limits the degree of melt-fragment quenching; and (3) the high superheat of the water, which on some occasions makes the steam released optically transparent instead of opaque, as is condensed or saturated volcanic steam from Surtseyan eruptions (Thorarinsson, 1966).

Rigorous scaling of the model's eruptive activity has not been attempted. Our efforts have thus far been directed at studying the feasibility of simulating volcanic explosions by this technique. Numerous experimental studies, including Board *et al.* (1975), Dullforce *et al.* (1976), Fröhlich *et al.* (1976), and Nelson and Duda (1981), have demonstrated the complexity of FCIs and have shown that explosive efficiencies may increase with system size. Therefore, scaling formulas have yet to be determined. To scale time for the model, we can compare the length dimension to that of Mount St. Helens to give a geometric scale, n. Approximately 0.5 km^3 of new lava erupted from Mount St. Helens on May 18, 1980. Our model uses about 5×10^{-2} m^3 of thermite that results in $n = 10^4$. Model times approximately scale by a factor of $n^{1/2}$ or about 10^2.

Four types of volcanic activity have been modeled and are described in Table 12.1. Strombolian activity results in fountaining of ejecta in ballistic trajectories over periods of minutes. Strong Surtseyan activity is short lived (less than 1 to 2 sec). Material is ejected in unsteady surging flow, and ballistic behavior of ejecta is minor or entirely absent. Weak Surtseyan activity is more steady, lasting for periods of 10 or more sec. Characteristics of both ballistic and surge movement of ejecta are observed. Finally, the fourth type of activity is passive quenching of the melt into lumps with little or no ejection into the atmosphere. Vulcanian activity (Mercali and Silvestri, 1891) can be compared with strong Surtseyan blasts that are very short lived or cannon-like. The hydromagmatic origin of Vulcanian activity has yet to be conclusively demonstrated. However, recent studies at Vulcano, Italy (Frazzetta *et al.*, 1983), and at Ngauruhoe, New Zealand (Nairn and Self, 1978; Self *et al.*, 1979), suggest the strong likelihood of meteoric water interaction in this eruptive style.

Ejecta Characterization

Observations of ejecta grain sizes show that the model's melt fragments become finer with increasing energy and violence of ejection. A quantitative analysis of ejecta sizes has not yet been completed, but photo documentation and recovery of

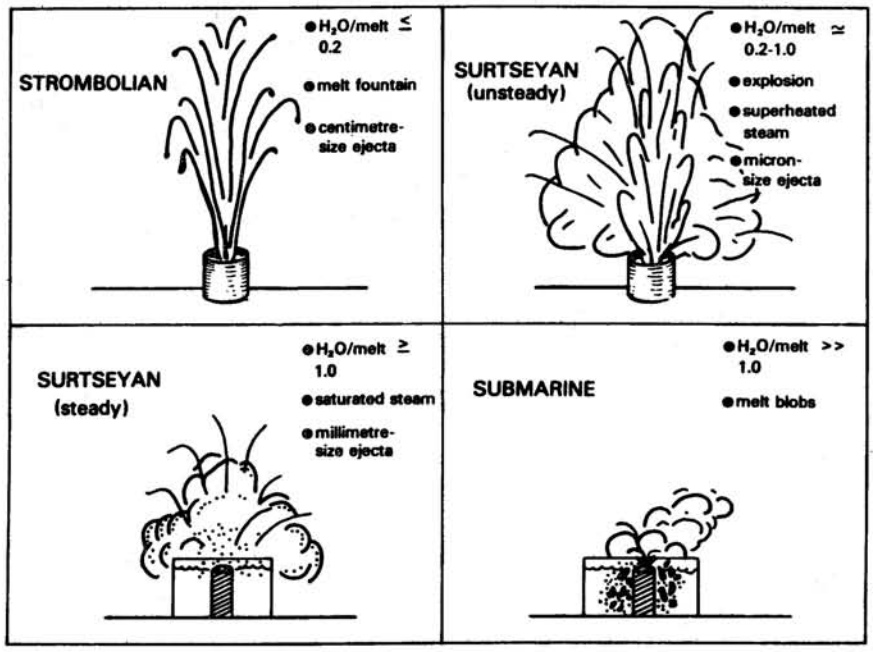

FIGURE 12.7 Summary of experimental results. Unsteady and steady Surtseyan activities are thought to produce tuff rings and tuff cones, respectively, as shown in Figure 12.2.

TABLE 12.1 Experimental Results

Experiment	R	Confinement	Description
Sand Burial			
1	0.23	0.5 m sand	Melt fragments of 1 to 2 mm in size fountained 2 to 3 m into the air for 4 to 5 sec; weak Strombolian.
2	0.13	0.5 m sand	Melt fragments of 1 cm in size fountained 7 to 10 m into the air for 2.5 sec; restricted neck vent; strong Strombolian.
Buried Confinement			
1	0.45	900 psi	Weak Surtseyan ejection of melt in less than 1 sec; eruption column 24 m high; horizontally moving base surge; 1-mm fragments; formed a tuff cone 2.5 m in diameter, 0.5 m high; continuous ejecta 5 m from rim.
2	0.22	900 psi	Strong Surtseyan blast lasting less than 1 sec; eruption column 40 m high; surge reaching 6 m from vent; submillimeter ejecta and accretionary lapilli; formed tuff ring 2.1 m in diameter, 0.27 m high; continuous ejecta 6 to 7 m from rim.
Water Box			
1	0.10-10.0	none	Variable access of H_2O to melt: Strombolian for several minutes with brief Surtseyan blasts (<1 sec), centimeter-size fragments ejected ballistically to a height of 10 m; Surtseyan blasts are brilliant hemispherically expanding clouds of micron-size particles in superheated steam; Surtseyan blast (<1 sec) destroying device, micron-size particles in horizontally directed surge.
2	0.10-10.0	none	Variable access of H_2O to melt: 50-sec Strombolian ballistic ejection of centimeter-size fragments with brief (<1 sec) Surtseyan sprays of submillimeter size particles; 60-sec, weak Surtseyan ejection of millimeter-size quenched melt fragments moving ballistically and in surges, saturated steam; submarine quenching of melt into millimeter- or centimeter-size lumps (pillows).
77-1	0.31	900 psi	Violent Surtseyan blast lasting less than 1 sec; eruption column 50 m high; micron-size dust carried away by wind.
77-2	0.23	900 psi	Surtseyan blast lasting 16 sec, 35 m in height, micron-size fragments, superheated steam; strong Strombolian eruption 90 sec long with two short Surtseyan blasts, centimeter-size fragments ejected ballistically; weak Strombolian fountain 10 m in height.
78-1	0.26	900 psi	Surtseyan 5-sec ejection of incandescent gas and micron-size particles 50 m high; pulsating Strombolian lasting 5 sec and weak Strombolian also of 5-sec duration; fountains up to 20 m high.
78-2	0.22	none	Surtseyan blast lasting 2 sec, micron-size fragments, and superheated steam jetted 40 m high; restricted vent.

fragmental debris permit a qualitative assessment. For Strombolian-type bursts, centimeter-size melt fragments are ballistically ejected and fall back around the vent. After strong Surtseyan explosions, little ejecta is noticeable around the volcano. Most of the ejecta is carried away as fine micron-sized dust (fine volcanic ash). Weak Surtseyan blasts are more steady in their ejection of material, as in the water-box experiments. Melt fragments are of millimeter size—roughly equivalent to coarse volcanic ash and lapilli. Passive quenching of the melt, analogous to formation of pillow lava, results in lumps or blobs of melt that range in size from millimeters to several centimeters.

Scanning electron microscopy (SEM) analyses of the explosive products (see Figure 12.8) reveal blocky-equant shapes, spheroidal and drop-like shapes, as well as irregular moss-like shapes (Wohletz, 1983). Thermite debris recovered from strong Surtseyan blasts ranges in median diameter from 1 to 40 μm, while less violent explosions produce debris with median diameters in the range of 100 to 200 μm. The size and shape of the melt fragments strongly resemble that of basaltic hydromagmatic ash studied by Heiken (1972) and Wohletz and Krinsley (1983).

Pressure Histories

Experimental pressure histories, presented in Figure 12.9, have been evaluated based on the magnitude and duration of pressure pulses. Strong Surtseyan activity generally is shown by off-scale (greater than 5000 psi or 350 MPa) response and short durations (several seconds or less). Weak Surtseyan activity also sends records off the scale, but durations may be up to 10 sec or more. Strombolian activity results in oscillating pressures from a few hundred psi to 1000-2000 psi. These oscillations are harmonic, with as many as 15 oscillations per second. If these oscillations are due to acoustic resonance, then sound speed for the system is about 10 m/sec, a value that agrees well with the values for liquid-gas mixtures calculated by Kieffer (1977). The Surtseyan blast of experiment 78-2 (Table 12.1) shows a

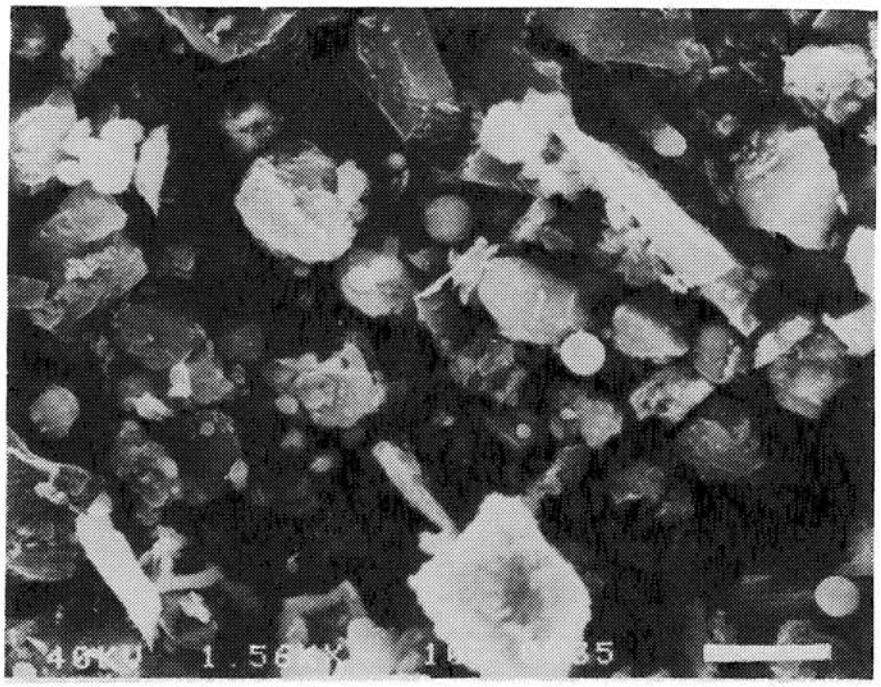

FIGURE 12.8 Scanning electron micrograph of some experimental explosion debris. Note the blocky equant grains and spherical shapes that strongly resemble basaltic volcanic ash particles. The debris is glassy and microcrystalline (undetermined mineralogy) and consists of dominantly Fe and Al oxides with subordinant amounts of SiO_2, TiO_2, MgO, MnO, Na_2O, CaO, and K_2O. The scale bar shown at the bottom of the photo is 10 μm, the average diameter of most grains pictured.

pressure buildup of only 400 psi, but the melt was completely ejected in less than 4 sec. Because no confinement valve was used, the low-pressure peak may be explained by lack of pressure buildup prior to ejection and an effectively larger orifice. The static pressure transducer used in experiment 77-2 (Table 12.1) recorded shock events characteristic of Surtseyan blasts. This record supports a theory developed by Board *et al.* (1975) of shock propagation during interaction of melt and water as well as observations of volcanic eruptions by Nairn (1976) and Livshits and Bolkhoritinov (1977).

DISCUSSION

The explosive energy of melt-water interaction is primarily manifested by the violence of melt ejection. The efficiency of an explosion is governed by several parameters. Four important controls are water-melt mass ratio, confining pressure, the amount of water superheating, and the degree of water-melt mixing.

Energy Calculations

Rough estimates of the mechanical energy developed in an explosive reaction can be obtained by analyzing the photographic record. Knowledge of the total mass of ejecta and the size of the vent orifice, coupled with estimates of the ejecta velocity history, can be used to determine a value for the system's kinetic energy. Pressure-time records are of a tremendous aid in this analysis. The ratio of kinetic energy to the initial thermal energy is the system's efficiency and a means by which to compare the relative explosivity of experiments.

A simpler way of estimating the thermal efficiency of these systems can be done by utilizing the known thermodynamics and a few simplifying assumptions. The first assumption required is that the actual method of heat exchange between the melt and the water is not important. Moreover, the melt and water need not be in thermal equilibrium; however, if equilibrium is not obtained, only minimum values of thermal efficiency are calculated. Known quantities are the specific volume, V, of the hot H_2O prior to ejection and the pressure, P, before expansion takes place. Recalling that the efficiency, E, of the system is

$$E = \frac{\text{work output}}{\text{heat input}} \tag{12.2}$$

and the heat, Q, equals the internal energy, U, plus the work, W

$$Q = U_f - U_i + W, \tag{12.3}$$

where f and i denote the final and initial states of the system. For thermodynamic systems where S denotes the entropy and T the temperature

$$dQ = dU + PdV \tag{12.4}$$

and

$$dU = TdS - PdV. \tag{12.5}$$

If the hot H_2O (steam) expands adiabatically to $P = 1$ atm, the work done on the steam is just

$$-W = U_f - U_i. \tag{12.6}$$

This calculation does not consider possible heat transfer to the steam during the expansion process, which would produce a greater thermal efficiency.

For the four experiments where pressure records were ob-

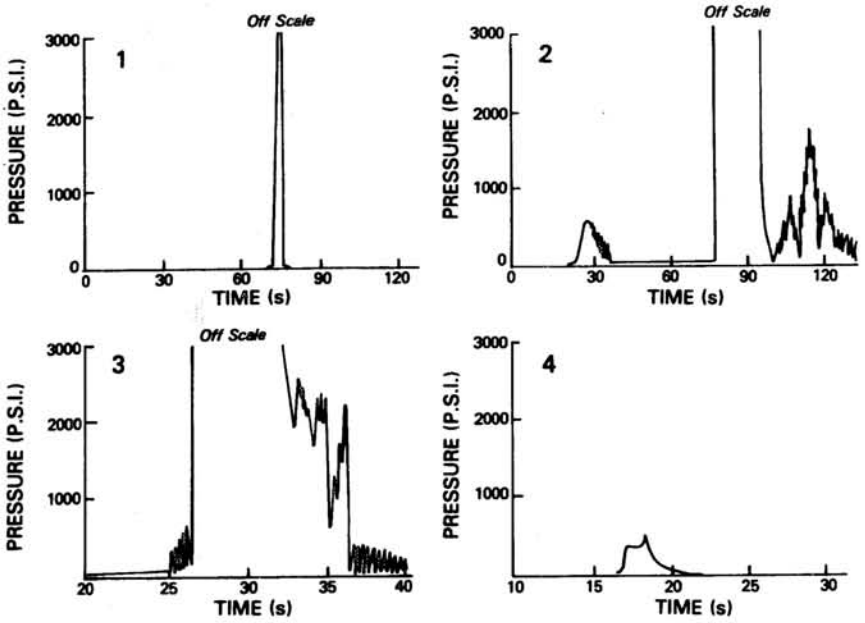

FIGURE 12.9 Pressure records for experiments 77-1, 77-2, 78-1, and 78-2 (Table 12.1), from which explosive efficiencies are calculated.

tained, 90 kg of thermite were used, which should have yielded approximately 7.9×10^4 kcal of heat input for the system. Specific volumes of the H_2O estimated from the system's geometry permit the use of steam tables to determine internal energies. The results of these calculations are given in Table 12.2 and show maximum efficiencies obtainable for the measured pressures.

Controls of Explosiveness

Figure 12.10 is a plot of thermodynamic efficiency versus water-melt ratio for four thermite experiments. It shows that efficiency increases with mass ratio. The relationship is nearly linear for the limited range of ratios tested. Experiment 78-2 (Table 12.1) plots below the line, probably because of the lack of confinement. The isobaric lines show the expected slope of the efficiency curve (at $T_{vapor} = 500°C$) for each mass ratio if efficiency is not pressure dependent. The fact that the experimental efficiency increases more quickly than simple isobaric extrapolations indicates that the heat-exchange mechanism itself becomes more efficient with increasing mass ratios.

Confinement is obtained in three ways: physical (lithostatic or hydrostatic), acoustic, and inertial. These mechanisms allow pressure to build up in the system and thus influence the heat-transfer efficiency. Physical confinement maintains the pressure until the burst limit is exceeded. Acoustic confinement is short lived but results in large localized dynamic pressures until unloading occurs. Unloading takes place after the pressure wave has traveled to a free surface and is reflected back as an expansion wave. In this way, large dynamic pressures may exist for a time, the length of which depends on the sound velocity and the dimensions of the system. Inertial confinement arises through the momentum of the melt and water. In our experiments the melt drops into the water. This impact provides the initial perturbation necessary for mixing.

Explosive heat transfer results in maximum pressure rise over a few milliseconds (Sandia Laboratories, 1975). More recent studies (Reid, 1976; Buxton *et al.*, 1980) indicate even shorter time scales, on the order of microseconds. These values depend, of course, on the system volume. Conductive heat transfer, which is primarily a function of surface area, dominates in this rapid process. The experiments indicate that the size of ejected melt fragments decreases with increasing explosive energy (efficiency). But the melt surface area increases with decreasing grain size; hence, fragmentation of the melt and its mixing with water are required for explosive interactions. Vaporization energy is partitioned into ejection and fragmentation modes. The fragmentation process increases the melt surface area, ensures intimate contact with water, and promotes high thermal-energy transfer. Mechanisms explaining the fragmentation process are based on the creation of an initial, localized, pressure perturbation because of the expansion and collapse of a vapor film at the melt-water interface (Corradini, 1980; Wohletz, 1983). If the magnitude of the perturbation is sufficient in size to fragment a small part of the melt and cause mixing of the two fluids, the process is repeated, thereby fragmenting greater portions of the melt. Mixing, which results in increased surface area, promotes successive perturbation pulses (on a milli- or microsecond time scale). The magnitude of each pressure perturbation determines whether the next one will be larger. If the magnitude increases, the system grows in energy transfer exponentially. In this way each pressure perturbation promotes larger volumes of mixing, finer fragmentation, and increased heat-transfer rates. The process is limited when pressure pulses explosively disrupt the whole system. This self-sustained mixing has been called autocatalytic or dynamic mixing (Colgate and Sigurgeirsson, 1973) and can increase the heat-transfer rate by at least three orders of magnitude over normal boiling (Witte *et al.*, 1970).

Temperature calculations based on equilibrium saturation

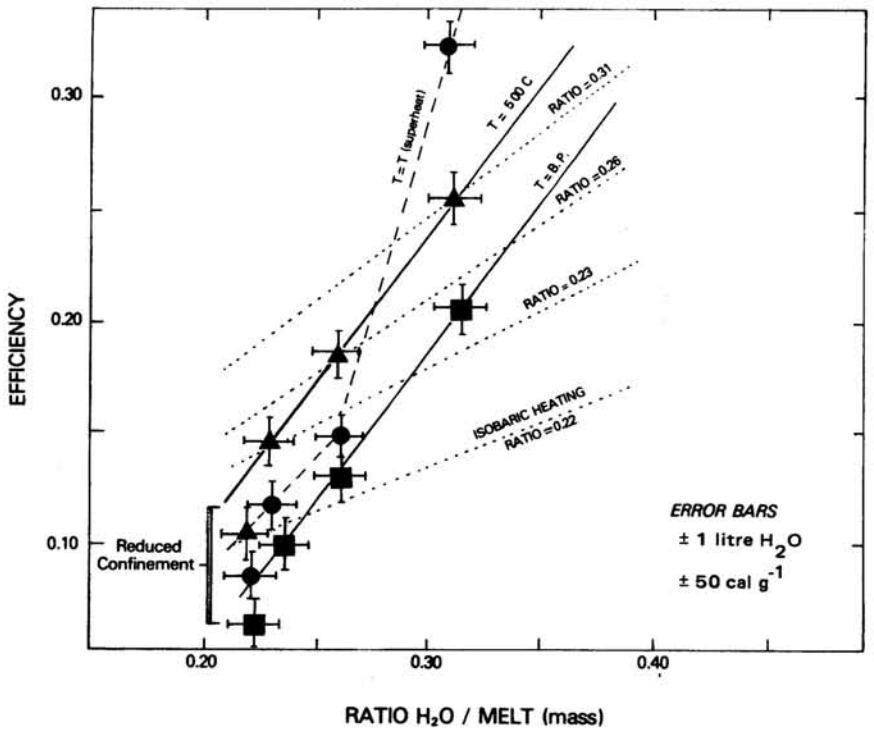

FIGURE 12.10 Plot of thermodynamic efficiency versus water-melt ratio. The solid lines connecting squares and triangles show efficiency curves for vaporization at the boiling point (BP) and for the added energy of heating vapor to 500°C, respectively. The dashed curve connecting dots shows efficiency of superheating. The dotted lines show isobaric extrapolations for efficiencies calculated at T = 500°C.

curve volumes are less than the minimum measured temperature of 500°C. This discrepancy and the molten nature of the ejecta indicate a possibility that thermal equilibrium is not reached at the explosion center. For nonequilibrium conditions water may be in the metastable state of superheat. Reid (1976) showed that superheating is to be expected, especially when a cold fluid is heated above its boiling point by a hot fluid. In the metastable state of superheating, where liquid water exists at temperatures well above its boiling point, the chemical potential for vaporization is less than that needed to overcome the confining pressure of the surrounding liquid. Many investigators (see Sandia Laboratories, 1975; Reid, 1976) have suggested that the limit of superheating, T_{sl} (the spontaneous nucleation temperature), is the temperature that water must reach for explosive vaporization.

Calculated efficiencies based on the limit of superheating are given in Table 12.2. For Experiment 77-1 (above $P_{crit.}$), T_{sl} is extrapolated along the line given by Reid (1976) to the point of intersection with the maximum isobar. Figure 12.10 is a plot of calculated efficiencies of superheating compared with nonsuperheating systems. Again, experiment 78-2 plots below the line. The curve demonstrates the added efficiency of superheated systems in which maximum efficiency may occur at mass ratios near 0.35 to 0.70. A tentative conclusion on the effect of confinement is that confinement appears to increase the efficiency of equilibrium systems. For nonequilibrium systems,

TABLE 12.2 Experimental Efficiency Calculations

Experiment	Mass H_2O (kg)	Mass Thermite (kg)	Ratio	Burst P (bars)[a]	Vapor T (°C)[a]	Superheat T (°C)[b]	Efficiency[c] (1)	(2)	(3)
77-1	28	90	0.31	350	426	710	0.20	0.25	0.32
77-2	21	90	0.23	1/2(210)	368	370			
				1/2(70)	284	344	0.10	0.14	0.11
78-1	22	90	0.26	3/4(210)	368	370			
				1/4(140)	335	359	0.12	0.18	0.14
78-2	20	90	0.22	28	228	336	0.06	0.10	0.08

[a] T and P are time averaged for experiments 77-2 and 78-1.

[b] Superheat, T, is calculated from Reid (1976).

[c] Efficiency is (1) for vaporization at the boiling point, (2) for the additional enthalpy of heating the vapor to 500°C, and (3) for the enthalpy of superheating.

confinement appears to promote superheating and increase the efficiency of those systems (Reid, 1976).

Applications to Geologic Systems

Previous studies (Sandia Laboratories, 1975) conclude that the most explosive interactions occur when $R < 1.0$, which is in agreement with our preliminary data. Figure 12.11 shows a schematic diagram of explosive efficiency versus water-melt ratio. Divisions for Strombolian, Surtseyan, and submarine activity are postulated from experiments and field studies (Wohletz, 1979; Wohletz and Sheridan, 1983). For basalt with a lower melt enthalpy, maximum yield would be near $R = 0.1$ to 0.3. The sharp slope increase in efficiency near $R = 0.1$ is due to the onset of superheating and explosive fragmentation. The gradual efficiency decrease at R near 1.0 is due to the quenching by excess volumes of water, which hinders development of high pressures and superheating and, hence, results in lower heat-transfer rates.

A limitation in application of this model to natural hydromagmatic systems involves the contact geometry of the melt with water. As mentioned earlier, contact geometry is a control of explosivity. The geometry affects the initial surface area of melt-water contact and the tendency of the melt to fragment during contact. This effect has been qualitatively observed in the various experimental designs. In natural systems, magma rises into a surface water body or a water-saturated country rock, as pictured in Figure 12.1. Other less-common situations of contact are discussed by Wohletz and Sheridan (1983). The case of a surface body of water is most closely modeled by our present experiments; however, the second case, that of water-saturated country rock, involves some complications. Sufficient mixing ratios are achieved generally where groundwater is concentrated along a fault. Magma rising along that fault forms a tabular shape that may expose enough surface area with the structurally trapped water to initiate small vapor explosions. If the country rock is incompetent, such as alluvium or sand, the small initial explosions excavate the fault zone, thereby increasing the magma-water contact area. Field studies (Wohletz and Sheridan, 1983) show that eruptions beginning this way start out as low-energy ejections of dominantly fragmented country rock and subordinate juvenile material. As the zone of mixing increases in size, eruptions progressively increase in intensity as a result of greater fluxes of water contacting the rising magma. By this process, eruptions evolve from low-energy Strombolian to high-energy Surtseyan explosions. This process also operates in reverse—as was the case for Surtsey. Initial contacts of magma and water on the ocean floor result in high water-melt ratios. As pillow lavas build up around the vent and attain levels near the surface of the sea, ratios decrease and Surtseyan activity results. Eventually, water no longer had access to the vent, and Strombolian activity with passive lava emplacement characterized final eruptions.

CONCLUSIONS

Interaction of a basalt-like melt with water varies in explosivity from passive quenching of the melt to highly energetic fragmentations. A spectrum of explosive phenomena may be experimentally produced and compared with different kinds of hydromagmatic activity, including Strombolian, Surtseyan, and submarine volcanic activity. Furthermore, experiments indicate that the nature of activity and its explosiveness is primarily controlled by the water-to-melt mass ratio and confining pressure. Varying contact geometries also control the nature of melt-water interaction and ejection mode.

Small amounts (less than 10 mass percent) of water contacting

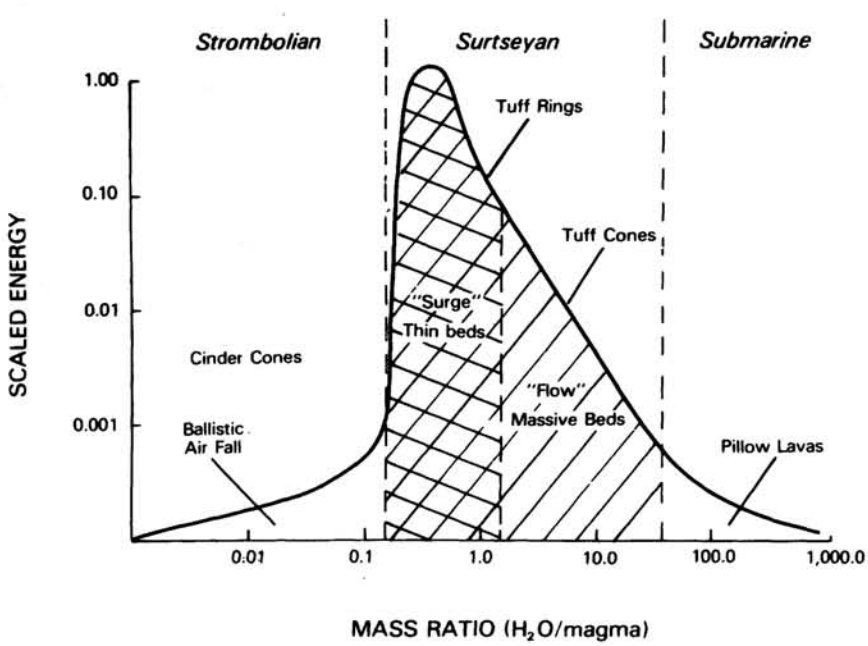

FIGURE 12.11 Plot of explosive energy versus water-melt ratio for volcanic systems. Energy is scaled to maximum yield. The sharp rise in the curve marks the onset of dynamic mixing and superheating. Surge eruptions are pulsating, high-energy, superheated steam explosions of dominantly fine ash. Flow eruptions are a more steady ejection of coarse tephra in saturated steam.

basalt produce Strombolian eruptions of dominantly centimeter-size fragments. Mass ratios of water and melt near 0.3 result in highly explosive Surtseyan blasts of millimeter and micron-sized material. Abundant amounts of water (greater than ratios of 2 or 3) generally result in passive chilling and the formation of pillow basalts.

Future experiments can be designed to model a variety of melt compositions, extending our results to more silicic compositions. Field studies (Sheridan and Wohletz, 1981; Sheridan *et al.*, 1981) show that hydromagmatic activity produces predictable eruption and ejecta transport phenomena depending on the amount of water present at the vent. Transport of pyroclastic material in water vapor is a function of the ejection rate, vapor-to-pyroclast ratio, and physical state of water in the ejecta cloud (saturated-condensing steam, superheated-expanding steam, and liquid water). These parameters can be experimentally varied, which provides a method for conducting similitude studies of ejecta emplacement. Studies could, for example, model the extent of blast or surge transport; emplacement of hot ejecta on ice, snow, or a standing body of water; topographic effects on ejecta flows; and development of geothermal systems in and around a volcanic vent.

This feasibility study has demonstrated the usefulness of these volcano simulation experiments. It is now apparent that the experiments can be documented better. In particular, our study has led to a new design (Wohletz and Sheridan, 1982), shown in Figure 12.12.

These new experiments are aimed at refining calculations for the efficiency curve and extending them over greater ranges of R. The new design allows quick restoration of the system after experimentation and use of smaller amounts (about 10 kg) of thermite. The vent is directed downward and the devise acts as a rocket that weighs about 250 kg. The mechanical energy is calculated as a function of the acceleration and vertical lift measured using high-speed cinematography (see Figure 12.13).

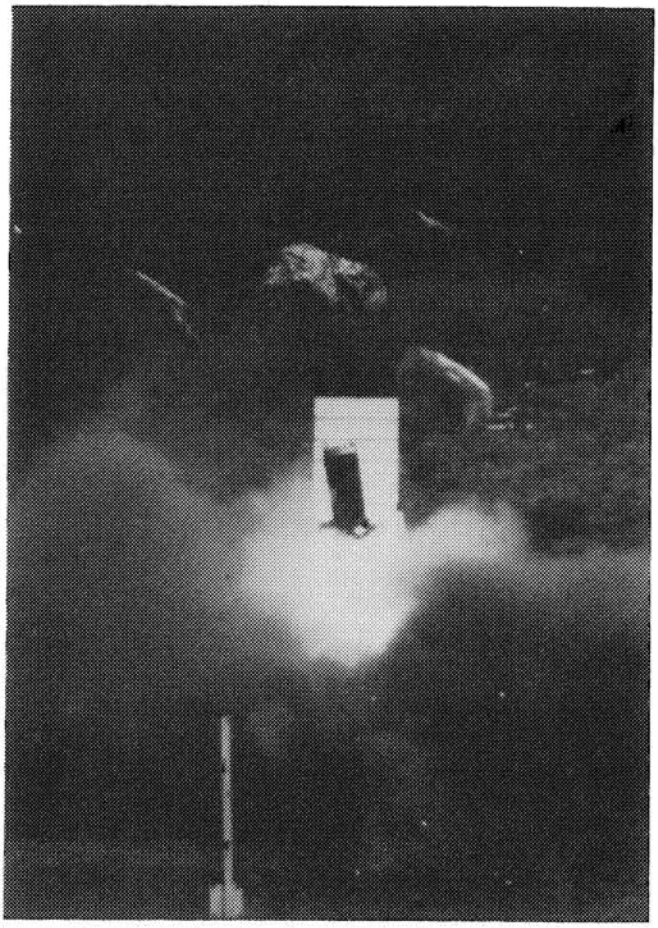

FIGURE 12.13 Experiment 80-5, series II, showing vertical lift as a measure of explosive energy.

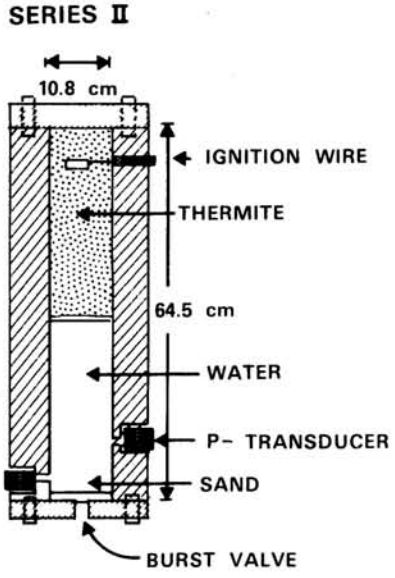

FIGURE 12.12 Series II experimental design for efficiency studies.

ACKNOWLEDGMENTS

This work was initiated following the enthusiastic recommendations of Thomas McGetchin. Technical support and materials were provided by the shock-wave physics group, M-6, at Los Alamos National Laboratory. Michael Sheridan helped with the applications to volcanic problems. NASA provided partial support through grants NSG-7642 and NAGW-245.

REFERENCES

Board, S. J., C. L. Farmer, and D. H. Poole (1974). Fragmentation in thermal explosions, *Int. J. Heat Mass Transfer 17*, 331-339.

Board, S. J., R. W. Hall, and R. S. Hall (1975). Detonation of fuel coolant explosions, *Nature 254*, 319-321.

Buxton, L. D., and W. B. Benedict (1979). Steam explosion efficiency studies, Sandia Laboratories, *SAND79-1399*, 62 pp.

Buxton, L. D., W. B. Benedict, and M. L. Corradini (1980). Steam explosion efficiency studies, part II, corium experiments, Sandia Laboratories, *SAND80-1324*, 36 pp.

Chouet, T. R., N. M. Hamicevicz, and T. R. McGetchin (1974). Photoballistics of volcanic jet activity at Stromboli, Italy, *J. Geophys. Res. 79*, 4961-4976.

Colgate, S. A., and Sigurgeirsson (1973). Dynamic mixing of water and lava, *Nature 244*, 552-555.

Corradini, M. L. (1980). Analysis and modelling of steam explosion experiments, Sandia Laboratories, *SAND80-2131*, 114 pp.

Dullforce, T. A., O. J. Buchanan, and R. S. Peckover (1976). Self-triggering of small-scale fuel-coolant interactions; I. Experiments, *J. Phys. Oil. Appl. Phys. 9*, 1295-1303.

Fisher, R. V., and A. C. Waters (1970). Base surge bed forms in maar volcanoes, *Am. J. Sci. 268*, 157-180.

Frazzetta, G., L. LaVolpe, and M. Sheridan (1983). Evolution of the Fossa cone, Vulcano, *J. Volcanol. Geotherm. Res. 17*, 329-360.

Fröhlich, A., A. Müller, and G. Unger (1976). Experiments with water and hot melts of lead, *J. Non-Equilib. Thermodyn. 1*, 91-103.

Heiken, G. H. (1972). Morphology and petrography of volcanic ashes, *Geol. Soc. Am. Bull. 83*, 1961-1988.

Jagger, T. A. (1949). *Steam Blast Volcanic Eruptions*, Hawaii Volcano Observ., 4th Spec. Rep., 137 pp.

Kieffer, S. W. (1977). Sound speed in liquid-gas mixtures: Water-air and water-steam, *J. Geophys. Res. 82*, 2895-2904.

Lipsett, S. G. (1966). Explosions from molten materials in water, *Fire Tech. (May)*, 118-126.

Livshits, L. D., and L. G. Bolkhoritinov (1977). Weak shock waves in the eruption column, *Nature 267*, 420-421.

McQueen, R. G., and K. H. Wohletz (in preparation). Experimental hydromagmatic volcanism.

Mercali, G., and O. Silvestri (1891). Le eruzioni dell'isola di volcano, incominciate il 3 Agosto 1888 e terminate il 22 Marzo 1890: Relazione Scientifica, 1891, *Ann. Uff. Cent. Meteor. Geodin. 10, No. 4*, 1-213.

Moore, J. G. (1967). Base surge in recent volcanic eruptions, *Bull. Volcanol. 30*, 337-363.

Nairn, I. A. (1976). Atmospheric shock waves and condensation clouds from Ngauruhoe explosive eruptions, *Nature 259*, 190-192.

Nairn, I. A., and S. Self (1978). Explosive eruptions and pyroclastic avalanches from Ngauruhoe in February 1975, *J. Volcanol. Geotherm. Res. 3*, 39-60.

Nelson, L. S., and P. M. Duda (1981). Steam explosion experiments with single drops of CO_2 laser-melted iron oxide, *Trans. Am. Nucl. Soc. 38*, 453-454.

Peckover, R. S., D. J. Buchanan, and D. E. Ashby (1973). Fuel-coolant interactions in submarine volcanism, *Nature 245*, 307-308.

Reid, R. C. (1976). Superheated liquids, *Am. Sci. 64*, 146-156.

Sandia Laboratories (1975). Core-meltdown experimental review, Sandia Laboratories, *SAND74-0382*, 472 pp.

Self, S., L. Wilson, and I. A. Nairn (1979). Vulcanian eruption mechanisms, *Nature 277*, 440-443.

Sheridan, M. F., and K. H. Wohletz (1981). Hydrovolcanic explosions, the systematics of water-tephra equilibration, *Science 212*, 1387-1389.

Sheridan, M. F., F. Barberi, M. Rosi, and R. Santacroce (1981). A model for plinian eruptions of Vesuvius, *Nature 289*, 282-285.

Thorarinsson, S. (1966). *Surtsey: The New Island in the North Atlantic*, Almenna Bokafelagid, Reykjavik, Iceland, 47 pp.

Walker, G. P. L., and R. Croasdale (1971). Characteristics of some basaltic pyroclastics, *Bull. Volcanol. 35*, 305-317.

Waters, A. C., and R. V. Fisher (1971). Base surges and their deposits, Capelinhos and Taal volcanoes, *J. Geophys. Res. 76*, 5496-5614.

Witte, L. C., J. E. Cox, and J. E. Bouvier (1970). The vapor explosion, *J. Metals 22*, 39-44.

Wohletz, K. H. (1979). Evolution of tuff cones and tuff rings, *Geol. Soc. Am. Abstr. Progr. 11*, 543.

Wohletz, K. H. (1983). Mechanisms of hydrovolcanic pyroclast formation: Size, shape, and experimental studies, *J. Volcanol. Geotherm. Res. 17*, 31-63.

Wohletz, K. H., and D. H. Krinsley (1983). Scanning electron microscope analysis of basaltic hydromagmatic ash, in *Scanning Electron Microscopy in Geology*, B. Whorley and D. Krinsley, eds., Geo Abstracts, Inc., Norwich, England.

Wohletz, K. H., and M. F. Sheridan (1981). Rampart crater ejecta: Experiments and analysis of melt-water interactions, *NASA Tech. Memo. 82325*, 134-135.

Wohletz, K. H., and M. F. Sheridan (1982). Melt-water interactions, series II, experimental design, *NASA Tech. Memo. 84211*, 169-171.

Wohletz, K. H., and M. F. Sheridan (1983). Hydrovolcanic explosions. II: Evolution of tuff rings and tuff cones, *Am. J. Sci. 283*, 385-413.